Available online at www.sciencedirect.com
ScienceDirect
Journal of The Franklin Institute 00 (2018) 1–17
Journal of The Franklin Institute

Adaptive Fuzzy Sliding Mode Command-Filtered Backstepping Control for Islanded PV Microgrid with Energy Storage System

Dezhi Xu[a,*], Yuchen Dai[b], Chengshun Yang[b], Xinggang Yan[c]

[a]*School of IoT Engineering (Institute of Electrical Engineering and Intelligent Equipment), Jiangnan University, Wuxi, 214122, China*
[b]*School of Electric Power Engineering, Nanjing Institute of Technology, Nanjing, 211167, China*
[c]*School of Engineering and Digital Arts, University of Kent, Canterbury, CT2 7NT, U.K.*

Abstract

This paper focuses on the control of islanded photovoltaic (PV) microgrid and designs a controller for PV system. Because of the system operates in islanded mode, the reference voltage and frequency of the AC bus are provided by the energy storage system. We mainly designed the controller for the PV system in this paper, and the control objective is to control the DC bus voltage and the output current of the PV system. Firstly, we set up a mathematical model of the PV system. In the design process of PV system controller, we use command-filtered backstepping control method to construct the virtual controller, and design the final controller by using sliding mode control. Considering the uncertainty of the circuit parameters in the mathematical model and the unmodeled part of the PV system, we have integrated adaptive control in the controller to realize on-line identification of component parameters of PV system. Meanwhile, we use fuzzy control to approximate the unmodeled part of the system. In addition, the projection operator guarantees the boundedness of adaptive estimation. Finally, the control effect of the designed controller is verified by MATLAB/Simulink software environment. By comparing with the control results of proportion-integral (PI) and other controllers, the advanced design of the controller is verified.

Keywords: Fuzzy control, command-filter backstepping, parameter adaptive, sliding mode, photovoltaic (PV), islanded operation mode.

1. Introduction

At present, the traditional fossil energy has dried up gradually, and renewable energy source has played an important role increasingly [1-2]. Photovoltaic (PV), as a kind of renewable energy source, has been widely applied [3-5]. PV power generation system can improve energy efficiency and power quality effectively, reduce carbon emissions and energy consumption, and enhance power system reliability [6-7]. Fig.1 shows the topology of the islanded microgrid we adopted. A PV power generation system can be composed of PV panels, maximum power point tracking (MPPT) equipment, DC/DC converter, voltage source converter (VSC), LC filter and transformer [8]. PV microgrid has two operation modes: grid connected and islanded mode [9]. This paper mainly focuses on the control of islanded PV microgrid. The PV microgrid operation in islanded mode can provide power for the load which away from the large power grid [10]. However, due to the islanded PV microgrid lacks of reference voltage and frequency provided

*Corresponding author
Email address: xudezhi@jiangnan.edu.cn, lutxdz@126.com (Dezhi Xu)

by external power grid, therefor, we need to add the main power source in the system to generate voltage and frequency reference in AC bus [11-12]. For the selection of the main power source, it can not be a kind of unstable power supply, such as PV panels or wind turbines. Thus, this paper selects energy storage system (ESS) as the main power source of islanded PV microgrid, providing reference voltage and frequency for AC bus. Due to the output power of the system is supplied to the load directly in islanded PV microgrid, it is worth noting that the output power of the PV system and the rated power of the load can not be exactly the same [13-14]. Therefore, the energy storage device not only provides the reference voltage and frequency for the system, but also can absorb the excess power generated by the PV system, and compensates the load power to achieve the rated power when the output power of the PV system is less than the rated power of the load [15]. In the control of ESS, we use V/f control strategy to stabilize the voltage and frequency of AC bus. This paper mainly designs a controller for the VSC in PV system to control the stability DC side bus voltage of VSC and the output active and reactive power of the system.

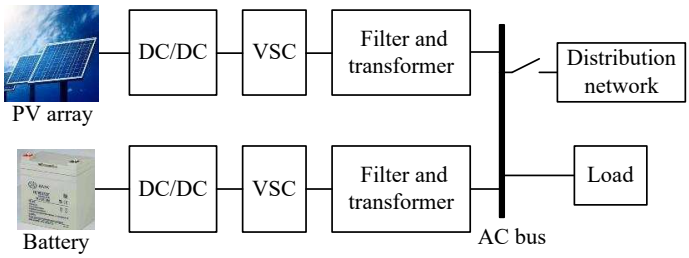

Figure 1: Topology of the islanded microgrid.

Many scholars have done some related work in improving the control effect of islanded microgrid. Reference [16] establishes the mathematical model for VSC in islanded microgrid, and a fractional-order sliding mode controller is designed for VSC. The designed controller realizes the tracking of the three-phase voltage to reference voltage at the end of the islanded microgrid. Therefore, the problem of no reference voltage and frequency in the islanded microgrid is solved. However, the article uses DC source instead of distributed energy resource, and the model established in this article is only suitable for some stable power sources. In addition, reference [16] also lacks consideration for the ESS. The work in [17] discusses the application of islanded PV system in cluster of house. In the article, the interconnection of multiple islanded microgrid is discussed, realizes the transmission of energy in multiple systems, and the energy storage system is connected to the AC side to achieve energy storage and release. But the author chose proportion-integral (PI) controller to control VSC. When the system is disturbed, it is difficult for the PI controller to show high robustness. Meanwhile, there is a lack of comparison with other control methods in this article. In reference [18], droop control is applied to the islanded AC-DC microgrid. AC bus and DC bus are supplied power to AC and DC loads respectively, and connected by interlinking converter. However, as in reference [17], the article also fails to compare the proposed control method with other control methods to demonstrate the advanced nature of the proposed control method. In reference [19], the voltage and frequency in the islanded system are controlled by fully decentralised control framework. This control method proposed is different from centralized and distributed control. The authors establish a sliding mode observer to estimate the information of other distributed generator units and verify the reliability of the method. However, this method must model the control object accurately, so the control strategy still needs improvement.

In recent years, advanced control has been applied in many engineering practices [20-22]. Advanced control includes predictive control, fuzzy control, neural control, nonlinear control and robust control et al, and it has better control effect than the traditional PI controller. From the section II, we know that the mathematical model we established is a second-order model. Thus, we construct the virtual controller by using backstepping control. Backstepping control is a kind of nonlinear control, and it is widely used in the control of higher-order models [23]. In order to reduce the differential process of the controller, we introduce the command-filter in the controller [24]. The work in [25] applies command-filtered backstepping control to nonlinear multi-agent tracking problems. The controller is designed and the stability of the system is verified based on Lyapunov stability theory. It can be seen from simulation that the designed controller has satisfactory control performance. In the model established for the PV system, the parameters of the resistance, inductance, and capacitance in the circuit are included. However, the measurement of these

parameters can not be very precise. Therefore, we consider the adaptive estimation of circuit parameters in the controller. In reference [26], a command-filtered backstepping controller is designed for compliant actuators robot arms with parameters estimation. The controller adaptively estimates the parameters while realizing the control objectives. From the simulation, it can be seen that the controller with the parameter adaptive controller reduces the chattering of the control torque compared with PI and sliding mode controller. Therefore, the performance of the controller is improved. In addition, we also take into account the incompleteness of the PV system model, the chattering can easily stimulate the unmodeled characteristics in the system. To solve this problem, we use fuzzy control to approximate the unmodeled part of the system and improve the performance of the controller [27-28]. We also introduce sliding mode control in the controller, which further increases the robustness of the controller [29].

In brief, this paper mainly design a adaptive fuzzy sliding mode command-filtered backstepping (DFSCB) controller for the PV system, which control the DC bus voltage and output power of the PV system. The chapters of this article are arranged as follows. In section II and III, we describe the topology of the whole system and derive the mathematical model of the PV system. In section IV, we elaborate the design flow of DFSCB controller. In section V, we build the simulation model and give the output waveform of the system. We summarized the full text and gave some conclusions in section VI.

2. Structure of the islanded microgrid with PV array and ESS

The structure of islanded microgrid with PV array and ESS is shown in Fig.2. The PV system and ESS are connected to the AC bus directly and supply the power to the load. In the PV system, we use PV array instead of DC source to simulate the actual operation of PV system. The whole system is in the islanded operation mode and it not connected to the external power grid.

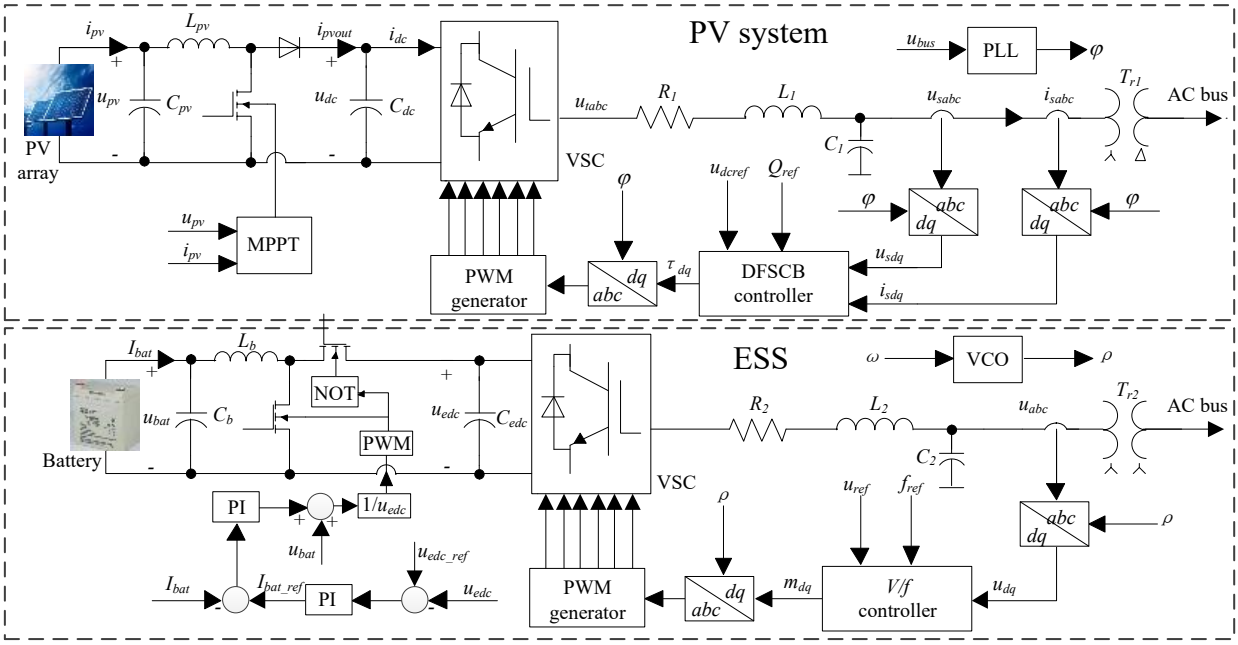

Figure 2: Structure of islanded microgrid with PV array and ESS.

2.1. The structure of ESS

As shown in Fig.2, in the design of the ESS topology of this article, we choose the battery as the energy storage equipment, and we define the ESS as the main power source of the whole system to provide reference voltage and frequency for the AC bus. In the DC side of the ESS, the battery is connected to the VSC through a two-way buck-boost circuit. The buck-boost circuit is controlled by PI control, the control objective is to increase the output voltage

of the battery and realize constant voltage charging and discharging. The flow chart of the control of the buck-boost circuit is included in Fig.2.

In the AC side of ESS, we use VSC to turn direct current into three-phase alternating current. Resistance R_2 represents the on state resistance of VSC, and inductance L_2, capacitance C_2 constitute the LC filter. The VSC in ESS is controlled by V/f controller. The reason why we choose the V/f controller is that we need to provide stable voltage and frequency for the AC bus in islanded microgrid. We specify the reference voltage and frequency for the V/f controller, and the controller realizes the tracking of the ESS output voltage and frequency to the given values. It is different from the PV system that the rotation angle ρ in ESS is provided by voltage controlled oscillator (VCO).

2.2. The structure of PV system

The controller of ESS is not what we want to discuss emphatically. We only use PI controller to realize the function of ESS. This article mainly discusses the design and performance improvement of PV system controller.

2.2.1. Structure of PV array

In our simulation, the equivalent circuit of PV cell is used to simulate the output characteristics of PV cell. The equivalent circuit of PV cell is shown in Fig.3. PV cell can be considered as a current source. According to Fig.3, the output current I of the PV cell has the following relations [30]:

$$I = I_{ph} - I_s\left(\exp\frac{q\,(U + IR_s)}{AkT} - 1\right) - \frac{U + IR_s}{R_{sh}}, \tag{1}$$

where I_{ph} is photo-generated current. q, k are the constants which $q = 1.602 \times 10^{-19}C$ and $k = 1.381 \times 10^{-23}J/K$. A and T are the characteristic coefficient of the diode and ambient temperature. It needs to be explained that the output current of a single PV cell is very small, so we make a number of PV cells in the simulation to make up the 100kW PV array to provide power for the system.

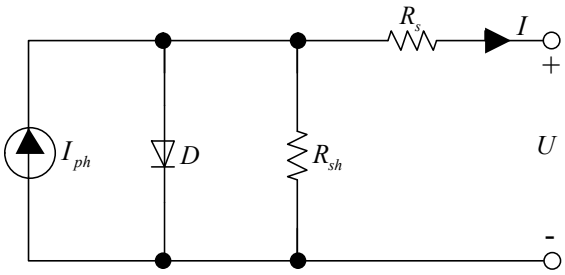

Figure 3: Equivalent circuit of PV cell.

2.2.2. Incremental conductance maximum power point tracking

As shown in Fig.4, the output voltage and power of the PV array are not linear when irradiance and temperature remain constant. Therefore, under fixed irradiance and temperature, there exists an output voltage U_{mp} corresponding to the maximum power P_{mp} output of PV array. For this point, we call the maximum power point (MPP). The MPP changes with the change of irradiance and temperature, and to tracking for the MPP is realized by incremental conductance maximum power point tracking (MPPT) controller.

From Fig.4, we know that the derivative of P-U curve is 0 at MPP. The incremental conductance MPPT algorithm is calculated as follows [30]. The output power P of the PV array in Fig.3 can be expressed as:

$$P = UI. \tag{2}$$

Find the derivative of equation (2), one obtains:

$$\frac{dP}{dU} = I + U\frac{dI}{dU}. \tag{3}$$

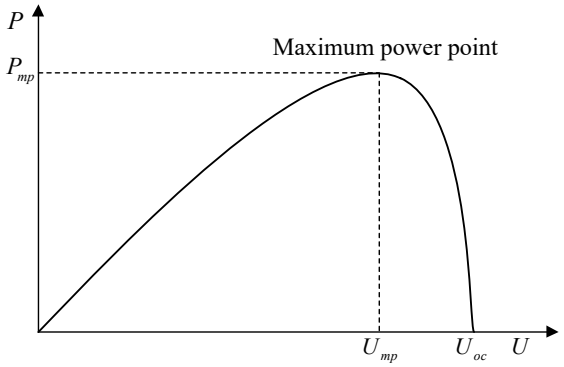

Figure 4: P-U curve of PV cell.

When (3) is equal to 0, the U at this time is the voltage corresponding to MPP, which expressed as:

$$I + U\frac{\Delta I}{\Delta U} = 0. \tag{4}$$

2.2.3. AC side

Similarly, we use VSC to connect the DC side and the AC side. R_1 represents the turn-on resistance of VSC, L_1 and C_1 constitute the LC filter. u_{tabc}, u_{abc} and i_{abc} are the three-phase terminal voltage of VSC and PV system and the three-phase output current, respectively. The DFSCB controller is designed in dq-frame, therefore, we converted the three-phase variables u_{sabc} and i_{sabc} to the dq-frame and provide to the controller. Because of the voltage and frequency of the AC bus is controlled by ESS, thus the rotation angle φ is provided by phase locked loop (PLL), which is the same as the rotation angle in AC bus. Modulation signals τ_d and τ_q in dq-frame is produced by DFSCB controller, then, the signals τ_d and τ_q are converted to the abc-frame to form three-phase modulation wave τ_{abc}. Finally, we use 10kHz triangular wave and three-phase modulation wave τ_{abc} to generate six-pulse signals to control VSC, so as to achieve control objectives.

3. Dynamic mode of PV system and fuzzy algorithm

3.1. Dynamic mode of PV system

The dynamic model of PV system is established in this section. From PV system in Fig.2, by using Kirchhoff's voltage law, the three-phase voltage and current in the system has the following relationship:

$$L_1\frac{d\vec{i_s}}{dt} = -R_1\vec{i_s} - \vec{u_s} + \vec{u_t}, \tag{5}$$

where vector $\vec{i_s}$, $\vec{u_t}$ and $\vec{u_s}$ are the space vector of the three phase variable i_{sabc}, u_{tabc} and u_{sabc}.Furthermore, the terminal voltage of the VSC $\vec{u_t}$ can be expressed as $\vec{u_t} = (u_{dc}/2)\vec{\tau}$, where $\vec{\tau}$ is the three-phase PWM modulating wave. So equation (5) can be rewritten as:

$$L_1\frac{d\vec{i_s}}{dt} = -R_1\vec{i_s} - \vec{u_s} + \frac{u_{dc}}{2}\vec{\tau}. \tag{6}$$

Then, convert equation (6) to dq-frame from abc-frame, one obtains:

$$\frac{di_{sd}}{dt} = -\frac{R_1}{L_1}i_{sd} + \omega i_{sd} - \frac{u_{sd}}{L_1} + \frac{u_{dc}}{2L_1}\tau_d, \tag{7}$$

$$\frac{di_{sq}}{dt} = -\frac{R_1}{L_1}i_{sq} - \omega i_{sq} - \frac{u_{sq}}{L_1} + \frac{u_{dc}}{2L_1}\tau_q. \tag{8}$$

According to the power conservation theorem (ignoring the impedance of C_{dc}, VSC, and LC filter), the power in the system has the following relation[31]:

$$u_{dc}i_{pvout} = \frac{3}{2}(u_{sd}i_{sd} + u_{sq}i_{sq}), \tag{9}$$

where i_{pvout} in Fig.2 represents the output current of the buck-boost circuit. Then, the calculation of the current relation at the capacitance C_{dc} is calculated as:

$$C_{dc}\frac{du_{dc}}{dt} = i_{pvout} - i_{dc}. \tag{10}$$

As a result, by combining (9) and (10), we can get the following relation:

$$\frac{du_{dc}}{dt} = \frac{3(u_{sd}i_{sd} + u_{sq}i_{sq})}{2C_{dc}u_{dc}} - \frac{i_{dc}}{C_{dc}}. \tag{11}$$

Integrating the equation (11), (7), and (Cq), we get the basic mathematical model of PV system. In the design of controller, we consider the adaptive estimation of unmodeled part and parameter. Therefore, the mathematical model of PV system is rewritten as follows:

$$\begin{aligned}
\frac{du_{dc}}{dt} &= \eta_1\left(\frac{3(u_{sd}i_{sd} + u_{sq}i_{sq})}{2u_{dc}} - i_{dc}\right) + \delta_1,\\
\frac{di_{sd}}{dt} &= -\eta_2 i_{sd} + \omega i_{sq} - \eta_3 u_{sd} + \eta_3\frac{u_{dc}}{2}\tau_d + \delta_2,\\
\frac{di_{sq}}{dt} &= -\eta_2 i_{sq} - \omega i_{sd} - \eta_3 u_{sq} + \eta_3\frac{u_{dc}}{2}\tau_q + \delta_3,
\end{aligned} \tag{12}$$

where $\eta_1 = 1/C_{dc}$, $\eta_2 = R_1/L_1$, $\eta_3 = 1/L_1$, and δ_1, δ_2, δ_3 represent the unmodeled nonlinear parts of the dynamic model of PV system.

3.2. Fuzzy algorithm

Fuzzy algorithm is applied in this paper to deal with the unmodeled part of PV system. Using the following fuzzy rules to construct a fuzzy system [32]:

$$IF\ x_1\ is\ A_1^{l_1}\ and \ldots and\ x_n\ is\ A_n^{l_n},\ Then\ u_d\ is\ S^{l_1\ldots l_n}, \tag{13}$$

where $l_1 = 1, 2, \ldots, m$, $i = 1, 2, \ldots, n$. The fuzzy controller can be calculated as:

$$f(x) = \frac{\sum_{i=1}^{N}\theta_i\prod_{j=1}^{n}\mu_j^i(x_j)}{\sum_{i=1}^{N}\prod_{j=1}^{n}\mu_j^i(x_j)} = \boldsymbol{\theta}^T\boldsymbol{\xi}(x), \tag{14}$$

where $\boldsymbol{\xi}(x) = [\xi_1(x), \xi_2(x), \ldots, \xi_N(x)]^T$, in whicn $\xi_i(x) = \frac{\prod_{j=1}^{n}\mu_j^i(x_j)}{\sum_{i=1}^{N}\prod_{j=1}^{n}\mu_j^i(x_j)}$, $\mu_j^i(x_j)$ is the membership degree of fuzzy system, and $\boldsymbol{\theta} = [\theta_1, \theta_2, \ldots, \theta_N]^T$ is the ideal constant weight vector.

According to the fuzzy universal approximation theorem, if $y(x)$ is defined as a function of compact set Ω, for any constant $\mu > 0$, there exists a fuzzy system satisfying $\sup_{f(x)\in\Omega} = |y(x) - f(x)| \le \mu$.

4. Design process of DFSCB controller

4.1. Controller design

In this section, we design the DFSCB controller m_d and m_q for the PV system in dq-frame. First of all, we approximate the unmodeled part by fuzzy function:

$$\delta_1 = \theta_1^T \xi_1(x),\ \ \delta_2 = \theta_2^T \xi_2(x),\ \ \delta_3 = \theta_3^T \xi_3(x). \tag{15}$$

We define $\tilde{\theta}_b = \hat{\theta}_b - \theta_b$ $(b = 1, 2, 3)$ as an estimated error, where $\hat{\theta}_b$ are the adaptive estimated value of θ_b, and $\hat{\delta}_b = \hat{\theta}_b^T \xi_b(x)$ are the fuzzy approximation value of δ_b.

For parameters η_a, $(a = 1, 2, 3)$, we define adaptive estimation error as $\tilde{\eta}_a = \hat{\eta}_a - \eta_a$, where $\hat{\eta}_a$ are the estimate of η_a.

Then, the tracking error of DC voltage is defined as:

$$e_1 = u_{dc} - u_{dcref}, \tag{16}$$

We choose the Lyapunov function as:

$$V_1 = \frac{1}{2} e_1^2, \tag{17}$$

and the derivative of V_1 can be calculated as:

$$\begin{aligned} \dot{V}_1 &= e_1 \dot{e}_1 = e_1 \left(\dot{u}_{dc} - \dot{u}_{dcref} \right) \\ &= -c_1 e_1^2 + e_1 \left(\eta_1 \left(\frac{3\left(u_d i_d + u_q i_q \right)}{2u_{dc}} - i_{dc} \right) + \theta_1^T \xi_1(x) - \dot{u}_{dcref} + c_1 e_1 \right) \end{aligned} \tag{18}$$

where $c_1 > 0$ is a designed constant. To stabilize V_1, and consider adaptive parameter estimation and fuzzy approximation, we choose the virtual controller as:

$$\hat{i}_{sd}^d = \frac{2u_{dc}}{3u_{sd}\hat{\eta}_1} \left(-c_1 e_1 - \hat{\theta}_1^T \xi_1(x) + \dot{u}_{dcref} + \hat{\eta}_1 i_{dc} \right) - \frac{u_{sq} i_{sq}}{u_{sd}}. \tag{19}$$

In order to reduce the computational complexity of the controller, we introduce an instruction filter in the controller, and the structure of the command-filter is shown in Fig.5.

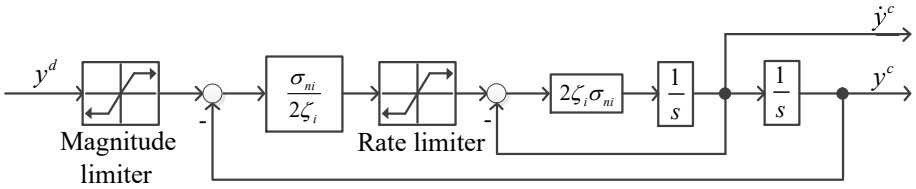

Figure 5: Structure of the command-filter.

The state equation of the command-filter can be written as [33]:

$$\begin{bmatrix} \dot{y}^c \\ \ddot{y}^c \end{bmatrix} = \begin{bmatrix} \dot{y}^c \\ 2\zeta_i \left[S_R \left(\frac{\sigma_{ni}}{2\zeta_i} \left(S_M(y^d) - y^c \right) \right) - \dot{y}^c \right] \end{bmatrix} \tag{20}$$

where y^d and y^c are the input and output signal of command-filter respectively, the waveform of the two signals should be the same. The σ_{ni} and ζ_i are the bandwidth and damping in the filter. If we design the virtual controller i_{sd}^d as the input of the command-filter, then we can get the derivative of virtual controller $\dot{i}_{sd}^c$ through integral part, thereby reducing the computation of the controller. The filtering error is defined as:

$$\dot{\varepsilon} = -c_1 \varepsilon + \frac{3u_{sd}\hat{\eta}_1}{2u_{dc}} \left(i_{sd}^c - i_{sd}^d \right). \tag{21}$$

7

Then, we redefine the DC voltage tracking error and the current tracking error in the system as:

$$\bar{e_1} = e_1 - \varepsilon,\ \ e_2 = i_{sd} - i_{sd}^c,\ \ e_3 = i_{sq} - i_{sq}^d, \tag{22}$$

and we need to redefine Lyapunov function to stabilize $\bar{e_1}$ simultaneously:

$$V_2 = \frac{1}{2}\bar{e_1^2}. \tag{23}$$

According to (18), (19), (21) and (22), the derivative of V_2 can be calculated as:

$$\begin{aligned}\dot{V}_2 &= \bar{e_1}\dot{\bar{e_1}} = \bar{e_1}\left(\dot{e}_1 - \dot{\varepsilon}\right)\\ &= -c_1\bar{e_1^2} + \frac{3u_{sd}\hat{\eta}_1}{2u_{dc}}\bar{e_1}e_2 - \tilde{\theta}^T\xi(x) + \tilde{\eta}_1\left(i_{dc} - \frac{3(u_{sd}i_{sd} + u_{sq}i_{sq})}{2u_{dc}}\right).\end{aligned} \tag{24}$$

We define the sliding mode surfaces in d-frame and q-frame as:

$$S_1 = k_1\bar{e_1} + e_2,\ \ S_2 = k_2e_2. \tag{25}$$

In order to facilitate the computation, we first seek the derivatives of S_1 and S_s as:

$$\begin{aligned}\dot{S}_1 &= k_1\dot{\bar{e_1}} + \dot{e}_2\\ &= k_1\dot{\bar{e_1}} + \left(\tilde{\eta}_2 - \hat{\eta}_2\right)i_{sd} + \omega i_{sq} + \left(\tilde{\eta}_3 - \hat{\eta}_3\right)u_{sd} + \left(\hat{\eta}_3 - \tilde{\eta}_3\right)\frac{u_{dc}}{2}\tau_d + \left(\hat{\theta}_2^T - \tilde{\theta}_2^T\right)\xi_2(x) - \dot{i}_{sd}^c,\end{aligned} \tag{26}$$

$$\begin{aligned}\dot{S}_2 &= k_2\dot{e}_3\\ &= k_2\left(\left(\tilde{\eta}_2 - \hat{\eta}_2\right)i_{sq} - \omega i_{sd} + \left(\tilde{\eta}_3 - \hat{\eta}_3\right)u_{sq} + \left(\hat{\eta}_3 - \tilde{\eta}_3\right)\frac{u_{dc}}{2}\tau_q + \left(\hat{\theta}_3^T - \tilde{\theta}_3^T\right)\xi_3(x) - \dot{i}_{sq}^c\right),\end{aligned} \tag{27}$$

where $k_1 > 0$, $k_2 > 0$ are the gains of the sliding mode surfaces.

In order to stabilize the entire system, we select the Lyapunov function once again as:

$$V_3 = V_2 + \frac{1}{2}S_1^2 + \frac{1}{2}S_2^2 + \frac{\tilde{\eta}_1^2}{2r_1} + \frac{\tilde{\eta}_2^2}{2r_2} + \frac{\tilde{\eta}_3^2}{2r_3} + \frac{\tilde{\theta}_1^T\tilde{\theta}_1}{2\lambda_1} + \frac{\tilde{\theta}_2^T\tilde{\theta}_2}{2\lambda_2} + \frac{\tilde{\theta}_3^T\tilde{\theta}_3}{2\lambda_3}, \tag{28}$$

where $r_a > 0, \lambda_b > 0, (a, b = 1, 2, 3)$ are the designed gains of adaptive law. Combination equation (24), (26) and (27), the derivative of V_3 can be calculated as:

$$\begin{aligned}\dot{V}_3 =& \bar{e_1}\dot{\bar{e_1}} + S_1\dot{S}_1 + S_2\dot{S}_2 + \frac{\tilde{\eta}_1\dot{\tilde{\eta}}_1}{r_1} + \frac{\tilde{\eta}_2\dot{\tilde{\eta}}_2}{r_2} + \frac{\tilde{\eta}_3\dot{\tilde{\eta}}_3}{r_3} + \frac{\tilde{\theta}_1^T\dot{\tilde{\theta}}_1}{\lambda_1} + \frac{\tilde{\theta}_2^T\dot{\tilde{\theta}}_2}{\lambda_2} + \frac{\tilde{\theta}_2^T\dot{\tilde{\theta}}_3}{\lambda_3}\\ =& -c_1\bar{e_1^2} + \frac{3u_{sd}\hat{\eta}_1}{2u_{dc}}\bar{e_1}e_2 - c_2S_1^2 - c_3S_1\mathrm{sat(S_1)} - c_4S_2^2 - c_5S_2\mathrm{sat(S_2)}\\ &+ S_1\left(k_1\dot{\bar{e_1}} - \hat{\eta}_2i_{sd} + \omega i_{sq} - \hat{\eta}_3u_{sd} + \hat{\eta}_3\frac{u_{dc}}{2}\tau_d + \hat{\theta}_2^T\xi_2(x) - \dot{i}_{sd}^c + c_2S_1 + c_3\mathrm{sat(S_1)}\right)\\ &+ k_2S_2\left(-\hat{\eta}_2i_{sq} - \omega i_{sd} - \hat{\eta}_3u_{sq} + \hat{\eta}_3\frac{u_{dc}}{2}\tau_q + \hat{\theta}_3^T\xi_3(x) - \dot{i}_{sq}^d + \frac{1}{k_2}c_4S_2 + \frac{1}{k_2}c_5\mathrm{sat(S_2)}\right)\\ &+ \frac{\tilde{\eta}_1}{r_1}\left(\dot{\hat{\eta}}_1 - r_1\bar{e_1}\left(\frac{3(u_{sd}i_{sd} + u_{sq}i_{sq})}{2u_{dc}} - i_{dc}\right)\right) + \frac{\tilde{\eta}_2}{r_2}\left(\dot{\hat{\eta}}_2 - r_2\left(-i_{sd}S_1 - k_2i_{sq}S_2\right)\right)\\ &+ \frac{\tilde{\eta}_3}{r_3}\left(\dot{\hat{\eta}}_3 - r_3\left(S_1\left(-u_{sd} + \frac{u_{dc}}{2}\tau_d\right) + k_2S_2\left(-u_{sq} + \frac{u_{dc}}{2}\tau_q\right)\right)\right)\\ &+ \frac{\tilde{\theta}_1^T}{\lambda_1}\left(\dot{\hat{\theta}}_1 - \lambda_1\left(\bar{e_1}\xi_1(x)\right)\right) + \frac{\tilde{\theta}_2^T}{\lambda_2}\left(\dot{\hat{\theta}}_2 - \lambda_2\left(S_1\xi_2(x)\right)\right) + \frac{\tilde{\theta}_3^T}{\lambda_3}\left(\dot{\hat{\theta}}_3 - \lambda_3\left(k_2S_2\xi_3(x)\right)\right),\end{aligned} \tag{29}$$

where c_2, c_3, c_4, $c_5 > 0$ are the designed controller parameters. According to equation (29), in order to ensure the convergence of the system, we design the controllers in d-frame and q-frame as:

$$\tau_d = \frac{2}{\hat{\eta}_3 u_{dc}}\left(-k_1\bar{e}_1 + \hat{\eta}_2 i_{sd} - \omega i_{sq} + \hat{\eta}_3 u_{sd} - \hat{\theta}_2^T \xi_2(x) + \dot{i}_{sd}^c - c_2 S_1 - c_3 \mathrm{sat}(S_1)\right), \tag{30}$$

$$\tau_q = \frac{2}{k_2\hat{\eta}_3 u_{dc}}\left(k_2\left(\hat{\eta}_2 i_{sq} + \omega i_{sd} + \hat{\eta}_3 u_{sq} - \hat{\theta}_3^T \xi_3(x) + \dot{i}_{sq}^d\right) - c_4 S_2 - c_5 \mathrm{sat}(S_2)\right). \tag{31}$$

The function sat(.) is the saturation function which expressed as:

$$\mathrm{sat}(S) = \begin{cases} 1, & S > \psi \\ S/\varphi, & |S| \le \psi \\ -1, & S < -\psi \end{cases} \tag{32}$$

where $0 < \psi \le 0.5$ is the layer of the sliding surface.

Still according to equation (29), the adaptive laws of entire system are designed as follows:

$$\begin{aligned}
\dot{\hat{\eta}}_1 &= r_1 \mathrm{Proj}\left(\hat{\eta}_1, \bar{e}_1\left(\frac{3(u_{sd}i_{sd} + u_{sq}i_{sq})}{2u_{dc}} - i_{dc}\right) - m_1\hat{\eta}_1\right), \\
\dot{\hat{\eta}}_2 &= r_2 \mathrm{Proj}\left(\hat{\eta}_2, \ -i_{sd}S_1 - k_2 i_{sq}S_2 - m_2\hat{\eta}_2\right), \\
\dot{\hat{\eta}}_3 &= r_3 \mathrm{proj}\left(\hat{\eta}_3, S_1\left(-u_{sd} + \frac{u_{dc}}{2}\tau_d\right) + k_2 S_2\left(-u_{sq} + \frac{u_{dc}}{2}\tau_q\right) - m_3\hat{\eta}_3\right), \\
\dot{\hat{\theta}}_1 &= \lambda_1 \mathrm{Proj}\left(\hat{\theta}_1, \bar{e}_1\xi_1(x) - n_1\hat{\theta}_1\right) \\
\dot{\hat{\theta}}_2 &= \lambda_2 \mathrm{Proj}\left(\hat{\theta}_2, S_1\xi_2(x) - n_2\hat{\theta}_2\right) \\
\dot{\hat{\theta}}_3 &= \lambda_3 \mathrm{Proj}\left(\hat{\theta}_3, k_2 S_2\xi_3(x) - n_3\hat{\theta}_3\right)
\end{aligned} \tag{33}$$

where $m_a > 0$, $n_b > 0 (a, b = 1, 2, 3)$ are the designed parameters. The function Proj(.) in (33) represents the projection operator (see in reference [34]), which guarantees that the adaptive parameter estimation is bounded.

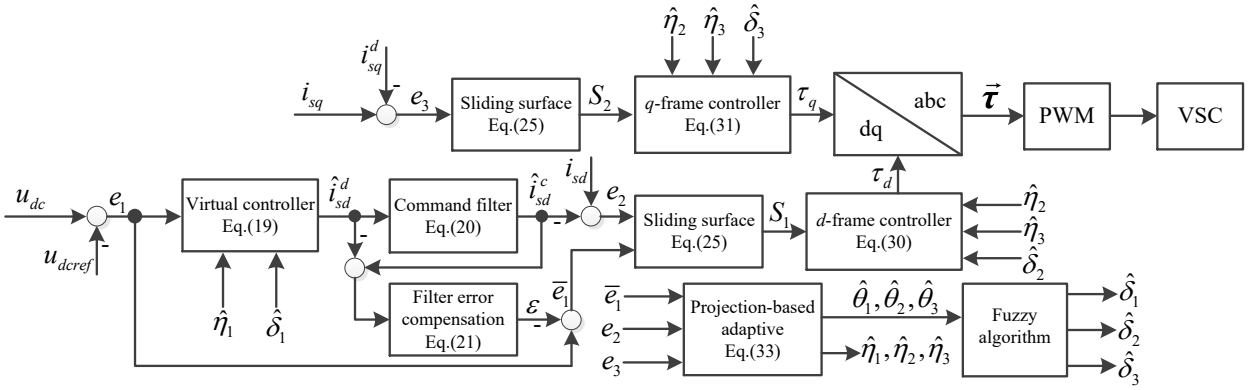

Figure 6: Signal flow diagram of the DFSCB controller.

4.2. Stability proof

Substituting (30), (31) and (33) into (29), the $\dot{V}_3$ is computed as:

$$\begin{aligned}
\dot{V}_3 = &-c_1\bar{e}_1^2 + \frac{3u_{sd}\hat{\eta}_1}{2u_{dc}}\bar{e}_1 e_2 - c_2 S_1^2 - c_3 S_1 \mathrm{sat}(S_1) - c_4 S_2^2 \\
&- c_5 S_2 \mathrm{sat}(S_2) - \sum_{a=1}^{3} m_a \frac{\tilde{\eta}_a^T \hat{\eta}_a}{r_a} - \sum_{b=1}^{3} n_b \frac{\tilde{\theta}_b^T \hat{\theta}_b}{\lambda_b}.
\end{aligned} \tag{34}$$

Define $0 < \mu < 1$, then from (34) we can obtain that $-c_1\bar{e}_1^2 + \frac{3u_{sd}\hat{\eta}_1}{2u_{dc}}\bar{e}_1 e_2 \le -c_1(1-\mu)\bar{e}_1^2 - c_1\mu|\bar{e}_1|^2 + \frac{3u_{sd}\hat{\eta}_1}{2u_{dc}}|\bar{e}_1||e_2|$. If we make $\frac{3u_{sd}\hat{\eta}_1}{2u_{dc}}|\bar{e}_1||e_2| - c_1\mu|\bar{e}_1|^2 \le 0$, that is $|\bar{e}_1| \ge \frac{3u_{sd}\hat{\eta}_1|e_2|}{2c_1\mu u_{dc}}$. then we can get the conclusion that $-c_1\bar{e}_1^2 + \frac{3u_{sd}\hat{\eta}_1}{2u_{dc}}\bar{e}_1 e_2 \le -c_1(1-\mu)\bar{e}_1^2$. Moreover, we can know that $c_3 S_1 \mathrm{sat}(S_1) \ge 0$, $c_5 S_2 \mathrm{sat}(S_2) \ge 0$ according to the definition in this article. Therefore, combining with the above conclusions, $\dot{V}_3$ has the following inequalities relationship:

$$\dot{V}_3 \le -c_1(1-\mu)\bar{e}_1^2 - c_2 S_1^2 - c_4 S_2^2 - \sum_{a=1}^{3} m_a \frac{\tilde{\eta}_a^T \hat{\eta}_a}{r_a} - \sum_{b=1}^{3} n_b \frac{\tilde{\theta}_b^T \hat{\theta}_b}{\lambda_b}. \tag{35}$$

Furthermore, according to the Young's inequality, we can obtain that:

$$\begin{aligned} -\tilde{\theta}_b^T\hat{\theta}_b &= -\tilde{\theta}_b^T\left(\tilde{\theta}_b + \theta_b\right) \le -\tilde{\theta}_b^T\tilde{\theta}_b + \frac{\tilde{\theta}_b^T\tilde{\theta}_b}{2} + \frac{\theta_b^T\theta_b}{2} \\ &\le -\frac{\tilde{\theta}_b^T\tilde{\theta}_b}{2} + \frac{\theta_b^T\theta_b}{2},\ (b = 1,2,3), \end{aligned} \tag{36}$$

similarly:

$$-\tilde{\eta}_a^T\hat{\eta}_a \le -\frac{\tilde{\eta}_a^T\tilde{\eta}_a}{2} + \frac{\eta_a^T\eta_a}{2},\ (a = 1,2,3), \tag{37}$$

Substituting equation (36) and (37) in (35), one obtains:

$$\begin{aligned} \dot{V}_3 \le\ & -c_1(1-\mu)\bar{e}_1^2 - c_2 S_1^2 - c_4 S_2^2 \\ & - \sum_{a=1}^{3}\left(\frac{m_a\tilde{\eta}_a^T\tilde{\eta}_a}{2r_a} - \frac{m_a\eta_a^T\eta_a}{2r_a}\right) - \sum_{b=1}^{3}\left(\frac{n_b\tilde{\theta}_b^T\tilde{\theta}_b}{2\lambda_b} - \frac{n_b\theta_b^T\theta_b}{2\lambda_b}\right) \\ \le\ & -\alpha V_3 + \beta \end{aligned} \tag{38}$$

where $\alpha = \min\{2c_1(1-\mu), 2c_2, 2c_4, m_a, n_b\}$, $a, b = 1,2,3$, $\beta = \sum_{a=1}^{3}\frac{m_a\eta_a^T\eta_a}{2r_a} + \sum_{b=1}^{a}\frac{n_b\theta_b^T\theta_b}{2\lambda_b}$.

As a result, we get the following conclusion from (38):

$$\begin{aligned} V_3(t) &\le \left(V_3(t_0) - \frac{\beta}{\alpha}\right)e^{-\alpha(t-t_0)} + \frac{\beta}{\alpha} \\ &\le V_3(t_0) + \frac{\beta}{\alpha},\ \forall t \ge t_0. \end{aligned} \tag{39}$$

In conclusion, it is proved that the system is bounded and stable. The signal flow diagram of the DFSCB controller is shown in Fig.6.

5. Simulation results and studies

In this section, we built the 100kW islanded PV power generation system with ESS in MATLAB/Simulink, see in Fig.7, and the whole simulation lasts 2s.

The circuit parameters in PV system and ESS are shown in Table I and II, the parameters of designed control laws are shown in Table III. The membership function of the fuzzy system is defined as: $\mu_j^i = \exp\left[-\left(x_j + l \times 2\right)^2/3\right]$, where $l = -5, -4, \cdots 0, \cdots, 5$, see in Fig.8.

In ESS, we make the output voltage of ESS to tracking the reference voltage (450V), and then raise the voltage through the transformer to stabilize the AC bus voltage at 20kV. In PV system, in order to observe the change of output power of PV system under different irradiance and temperature, the irradiance and temperature curves are given as shown in Fig.9. At $t = 1.6$s, irradiance and temperature remain stable.

Fig.10 illustrates the parameters adaptive estimation curves. As we can see from the Fig.10, the estimated curve fluctuates near the real value and presents a convergent trend. Fig.11 shows the fuzzy adaptive estimation curves. The estimation of the fuzzy system actually compensates for the dynamic changes of the system. It can be seen that the

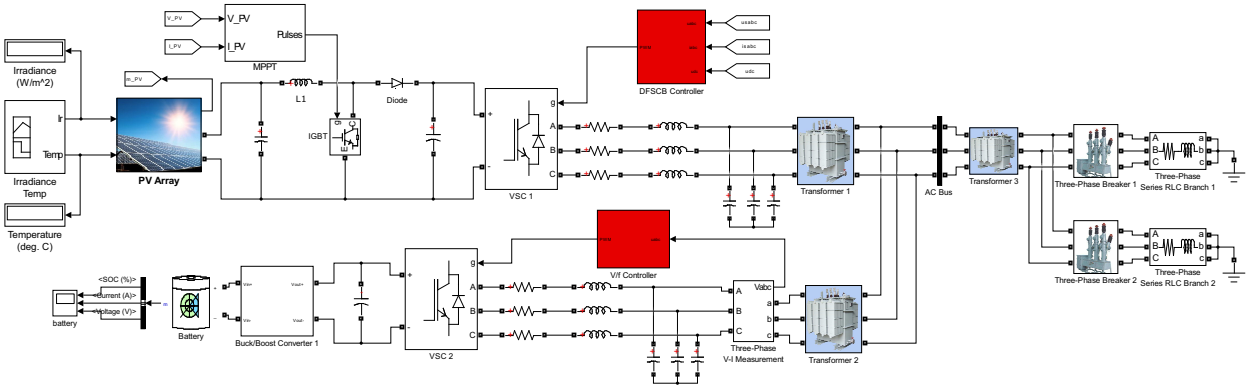

Figure 7: Simulation model of islanded PV microgrid with ESS.

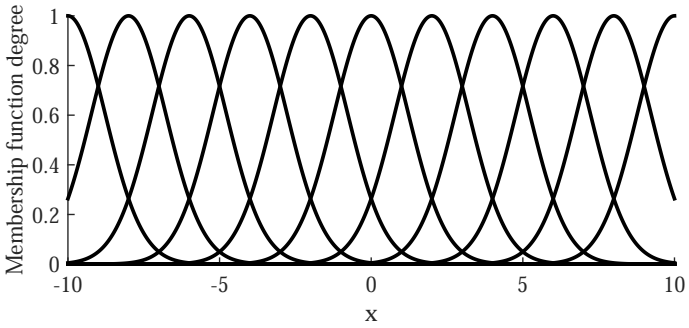

Figure 8: Membership function of fuzzy system.

Table 1: Parameters of PV system

Parameters	Value	Description
L_{pv}	5 mH	PV inductor
C_{pv}	100 μF	PV capacitance
C_{dc}	6 mF	DC-link capacitance
R_1	2 $m\Omega$	Filter resistance
L_1	250 μH	Filter inductor
C_1	500 μF	Filter capacitance
T_{r1}	0.26/25 kV/kV	Transformer ratio

fuzzy system has estimated the unmodeled part of the system, and has improved the performance of the system by matching with parameter adaptive.

Fig.12 illustrates the output active power waveform of PV system under different control methods. The controller in PV system intervened at t=0.05s. When t=0.4s, MPPT controller starts to work, and the system works at the MPP. When t=0.6s-1.6s, the output power varies with irradiation and temperature, and at t=1.6s-2s, the output power of the system is stable at 100kW. At t=0s-1.8s, the load is 42kW, at t=1.8s-2s, the load mutation to 128kW. It can be seen from Fig.12(a) that the output power under PI controller has large chattering, in addition, the load mutation has an impact on output power at t=1.8s. From Fig.12(b) we can see that the sliding mode command-filtered backstepping (SCB) controller has better performance than the PI controller, the output power curve under SCB controller is smoother than that under PI controller, but there is still chattering, moreover, when load mutated at t=1.8s, the impact

Table 2: Parameters of ESS

Parameters	Value	Description
L_b	1 mH	Battery inductor
C_b	150 μF	Battery capacitance
C_{edc}	6 mF	DC-link capacitance
R_2	3 $m\Omega$	Filter resistance
L_2	300 μH	Filter inductor
C_2	500 μF	Filter capacitance
ω	100π rad/s	Nominal angular frequency
T_{r2}	0.45/20 kV/kV	Transformer ratio

Table 3: Parameters of designed control laws

Parameters	Value	Description
c_1, c_2, c_3, c_4, c_5	1, 300, 360, 1200, 1000	Gains of DFSCB controller
r_1, r_2, r_3	30, 20, 5	Gains of adaptive laws
m_1, m_2, m_3	0.01, 0.01, 0.01	Gains of adaptive laws
λ_1, λ_2, λ_3	50, 100, 100	Gains of adaptive fuzzy laws
m_4, m_5, m_6	0.01, 0.01, 0.01	Gains of adaptive fuzzy laws
k_1, k_2	1.2, 1.2	Gains of sliding mode surface

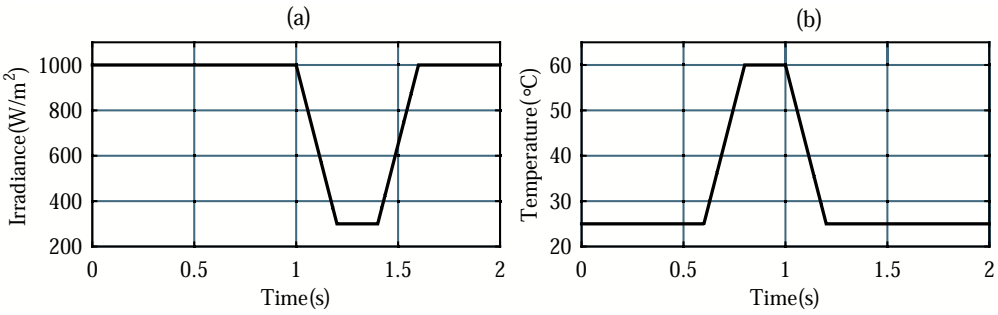

Figure 9: The curves of irradiance and temperature.

still exists. Fig.12(c) shows the output power curve under DFSCB controller. It can be seen that DFSCB has the best dynamic characteristics compared with PI and SCB controller. It is worth noting that parameters adaptive and fuzzy system further weaken the chattering of output power, and eliminate the effect of load switching on output power.

Fig.13(a) shows the load absorbed power, and Fig.13(b) shows the output power of ESS. The battery is absorbing excess power from the PV system when P_{bat} is negative, and when P_{bat} is positive, it represents that the PV system can not supply the rated power what load needed, and ESS discharge to compensates the power shortage. Fig.13(c) represents the state of charge (SOC) of the battery.

Fig.14 illustrates the DC bus voltage of PV system under DFSCB controller. Under the influence of the DFSCB controller, u_{dc} realizes the tracking of the given reference voltage u_{dcref} = 500V regardless of changes in irradiance and temperature. Fig.15 shows the three-phase voltage and current of AC bus at t=1.85-1.95 under DFSCB controller, under the control of the controller, the voltage and current are stabilized. Fig.16 shows the total harmonic distortion (THD) of AC bus current under PI, SCB and DFSCB controller. It can be seen that the current controlled by DFSCB controller has the minimum THD, which further verifies the control performance of the DFSCB controller.

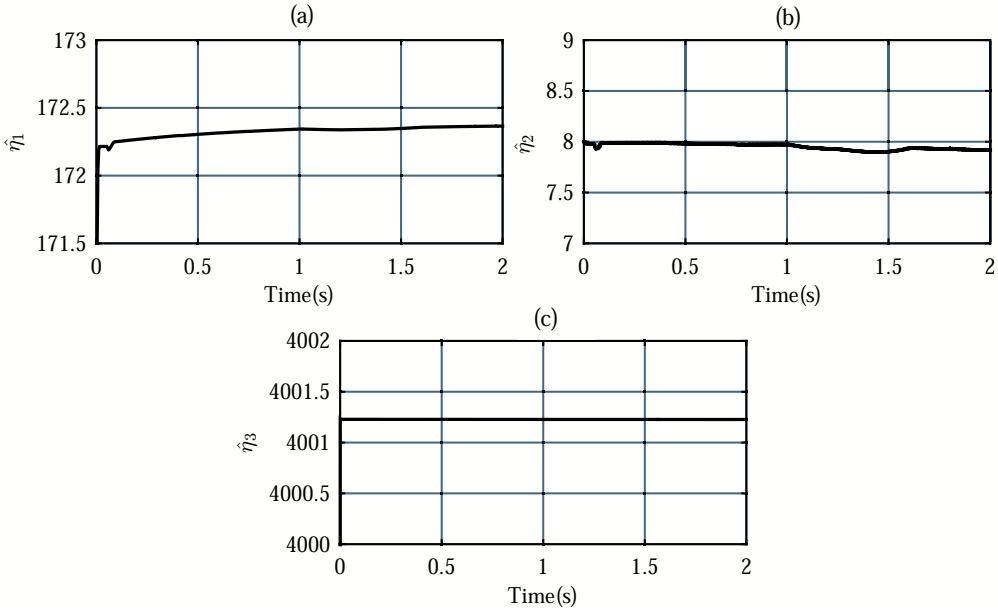

Figure 10: Parameters adaptive estimation curves.

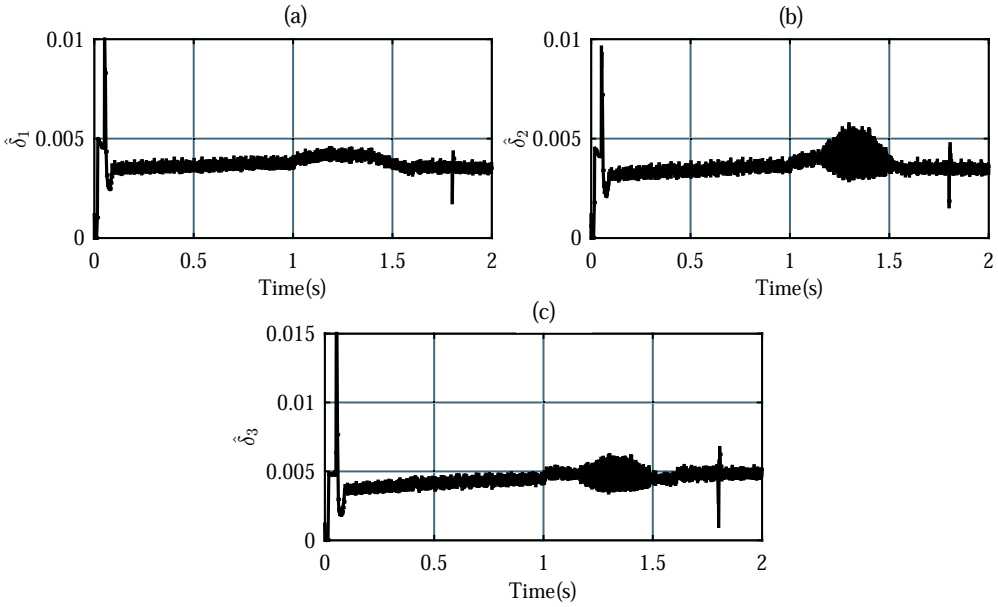

Figure 11: Fuzzy adaptive estimation curves.

6. Conclusion

In this paper, a 100kW PV system with ESS has been established in MATLAB/Simulink environment software. In the VSC in ESS, we adopted traditional PI based V/f controller to stabilize AC bus voltage, and provide reference voltage and frequency for PV system. Meanwhile, ESS implements the storage and release of energy. We mainly designed the DFSCB controller for PV system. DFSCB controller based on backstepping control method, and we introduce the command-filter to eliminate the differential expansion of traditional backstepping control. In order to increase the robustness of the system, we also introduce sliding mode control in the controller. In addition, to increase

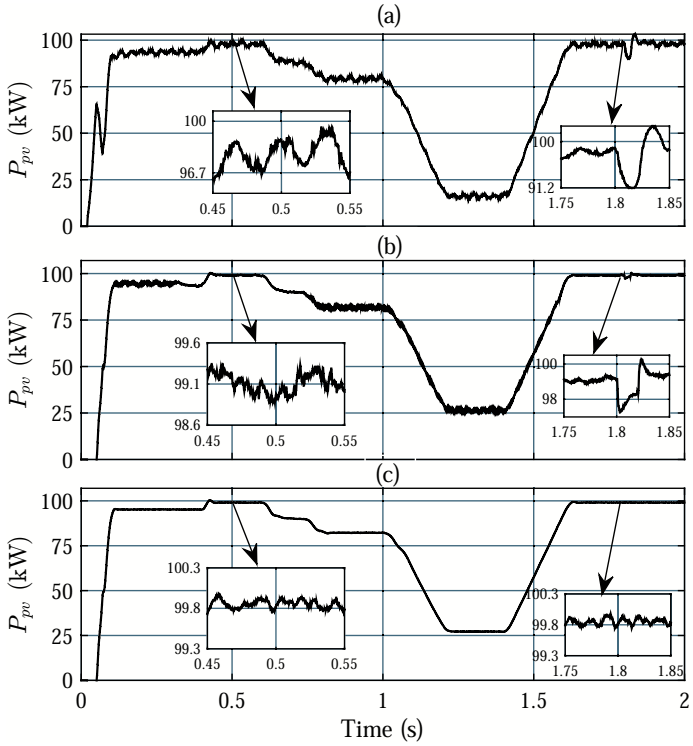

Figure 12: Output active power curve of PV system (a) under PI control, (b) under SCB control, (c) under DFSCB control.

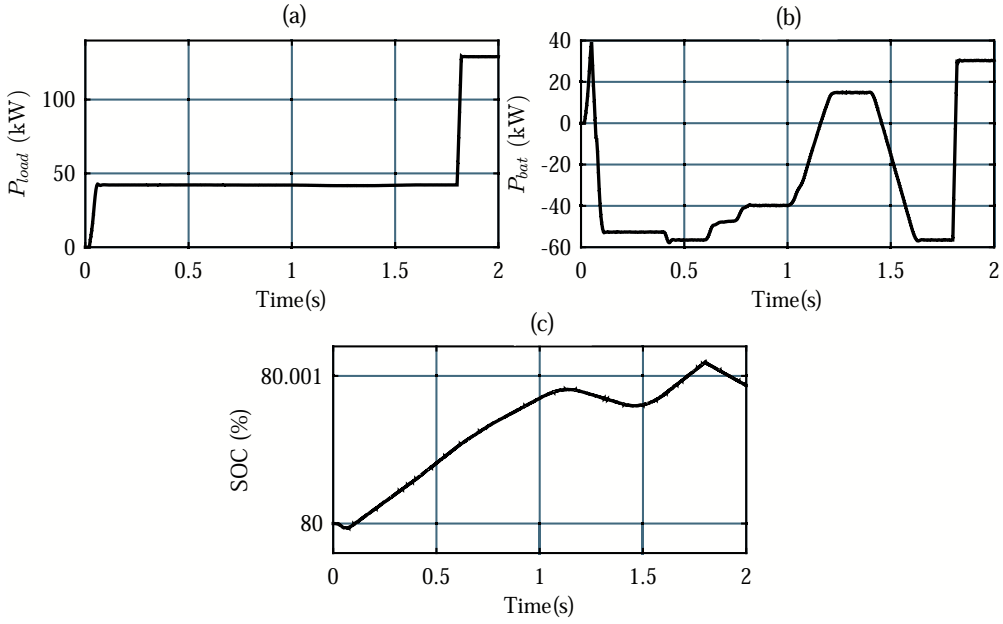

Figure 13: (a) The power absorbed by the load, (b) output power of ESS, (c) the SOC of battery.

the dynamic characteristics of the system, we consider the adaptive estimation of the parameters. Furthermore, to reduce the influence of the unmodeled part of the system on the control effect, we use fuzzy function to approximate

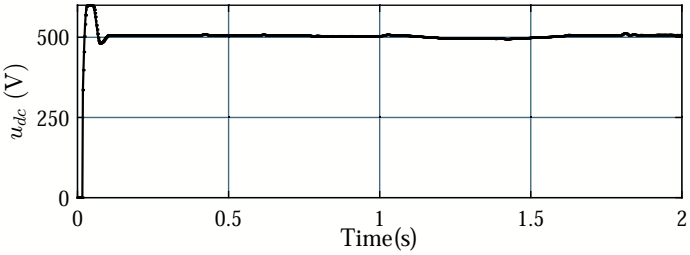

Figure 14: DC bus voltage of PV system under DFSCB controller.

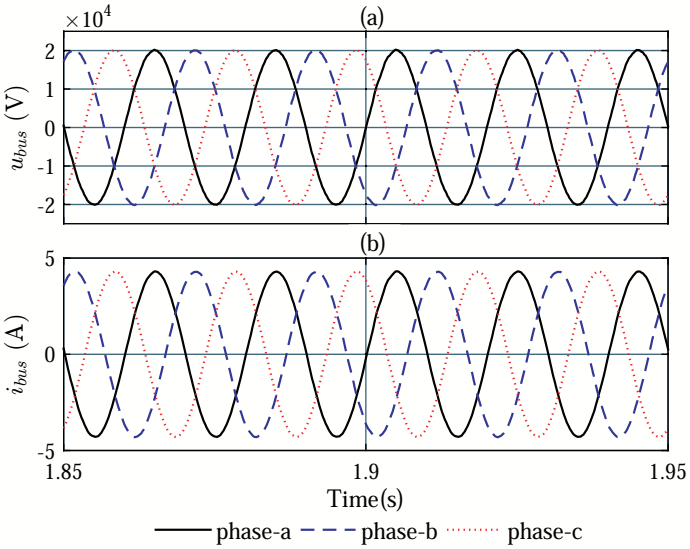

Figure 15: Three-phase (a) voltage and (b) current of AC bus under DFSCB controller.

the unmodeled part of the system. The simulation results show that the system under DFSCB controller has better dynamic characteristics and higher power quality compared with PI and SCB controller.

Acknowledgment

This work is supported by National Natural Science Foundation of China (61503156, 61403161, 61473250) and National Key Research and Development Program (2016YFD0400300) and Open Research Fund of Jiangsu Collaborative Innovation Center for Smart Distribution Network, Nanjing Institute of Technology (XTCX201714). The authors sincerely thank the editor and all the anonymous reviewers for their valuable comments and suggestions.

References

[1] B. M. Eid, N. A. Rahim, J. Selvaraj, et al, "Control methods and objectives for electronically coupled distributed energy resources in microgrids: a review", *IEEE Systems Journal*, 2016, 10(2): 446-458.

[2] D. Lew, M. Asano, J. Boemer, et al, "The power of small: the effects of distributed energy resources on system reliability", *IEEE Power and Energy Magazine*, 2017, 15(6): 50-60.

[3] Y. K. Wu, J. H. Lin and H. J. Lin, "Standards and guidelines for grid-connected photovoltaic generation systems: a review and comparison", *IEEE Transactions on Industry Applications*, 2017, 53(4): 3205-3216.

[4] P. Li, X. Yu, J. Zhang and Z. Yin, "The H_∞ control method of grid-tied photovoltaic generation", *IEEE Transactions on Smart Grid*, 2015, 6(4): 1670-1677.

[5] C. Kuo, J. Chen, S. Chen, et al, "Photovoltaic energy conversion system fault detection using fractional-order color relation classifier in microdistribution systems", *IEEE Transactions on Smart Grid*, 2017, 8(3): 1163-1172.

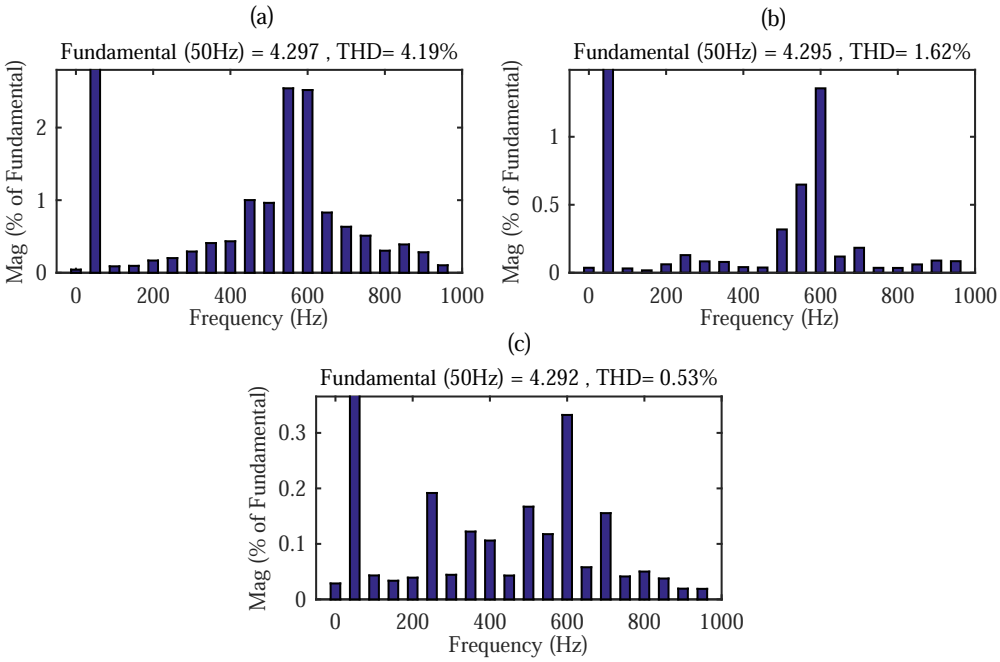

Figure 16: THD of AC bus current (a) under PI controller, (b) under SCB controller, (c) under DFSCB controller.

[6] X. Liu, M. Shahidehpour, Y. Cao, et al, “Microgrid risk analysis considering the impact of cyber attacks on solar PV and ESS control systems”, *IEEE Transactions on Smart Grid*, 2017, 8(3): 1330-1339.
[7] M. E. Ba?o?lu and B. ?ak?r, “Hybrid global maximum power point tracking approach for photovoltaic power optimisers”, *IET Renewable Power Generation*, 2018, 12(8): 875-882.
[8] F. Jaramillo-Lopez, G. Kenne and F. Lamnabhi-Lagarrigue, “Adaptive Control for a Class of Uncertain Nonlinear Systems: Application to Photovoltaic Control Systems”, *IEEE Transactions on Automatic Control*, 2017, 62(1): 393-398.
[9] J. Li, Y. Liu and L. Wu, “Optimal operation for community-based multi-party microgrid in grid-connected and islanded modes”, *IEEE Transactions on Smart Grid*, 2018, 9(2): 756-765.
[10] M. Cucuzzella, G. P. Incremona and A. Ferrara, “Decentralized sliding mode control of islanded AC microgrids with arbitrary topology”, *IEEE Transactions on Industrial Electronics*, 2017, 64(8): 6706-6713.
[11] L. G. Meegahapola, D. Robinson, A. P. Agalgaonkar, et al, ”Microgrids of commercial buildings: strategies to manage mode transfer from grid connected to islanded mode”, *IEEE Transactions on Sustainable Energy*, 2014, 5(4): 1337-1347.
[12] S. Sajadian and R. Ahmadi, “Model Predictive Control of Dual-Mode Operations Z-Source Inverter: Islanded and Grid-Connected”, *IEEE Transactions on Power Electronics*, 2018, 33(5): 4488-4497.
[13] D. Wu, F. Tang, T. Dragicevic, et al, “Autonomous Active Power Control for Islanded AC Microgrids With Photovoltaic Generation and Energy Storage System”, *IEEE Transactions on Energy Conversion*, 2014, 29(4): 882-892.
[14] J. Y. Kim, J. H. Jeon, S. K. Kim, et al., “Cooperative Control Strategy of Energy Storage System and Microsources for Stabilizing the Microgrid during Islanded Operation”, *IEEE Transactions on Power Electronics*, 2010, 25(12): 3037-3048.
[15] D. Wu, F. Tang, T. Dragicevic, et al, “A Control Architecture to Coordinate Renewable Energy Sources and Energy Storage Systems in Islanded Microgrids”, *IEEE Transactions on Smart Grid*, 2015, 6(3): 1156-1166.
[16] M. B. Delghavi, S. Shoja-Majidabad and A. Yazdani, “Fractional-order sliding-mode control of islanded distributed energy resource systems”, *IEEE Transactions on Sustainable Energy*, 2016, 7(4): 1482-1491.
[17] R. R. Jha, S. C. Srivastava and M. Kumar, “Development of control schemes for a cluster of PV-integrated houses in islanded mode”, *IET Renewable Power Generation*, 2017, 11(7): 903-911.
[18] V. Mortezapour and H. Lesani, “Adaptive primary droop control for islanded operation of hybrid ACCDC MGs”, *IET Generation, Transmission & Distribution*, 2018, 12(10): 2388-2396.
[19] G. Lou, W. Gu, L. Wang, et al, “Decentralised secondary voltage and frequency control scheme for islanded microgrid based on adaptive state estimator”, *IET Generation, Transmission & Distribution*, 2017, 11(15): 3683-3693.
[20] J. X. Ouyang, M. Y. Li, T. Tang, “Advanced control strategy and its controllable area for doubly fed wind farm integrated into power systems with VSC-HVDC transmission under grid fault”, *The Journal of Engineering*, 2017, 2017(13): 1170-1175.
[21] Z. Zhang, J. Rodrłguez and R. Kennel, “Advanced control strategies for direct-drive PMSG wind turbine systems: Direct predictive torque control approaches”, *CPSS Transactions on Power Electronics and Applications*, 2017, 2(3): 217-225.
[22] Y. Shi, C. Shen and H. Fang, “Advanced Control in Marine Mechatronic Systems: A Survey”, *IEEE/ASME Transactions on Mechatronics*, 2017, 22(3): 1121-1131.
[23] L. Wang, L. Cao and L. Zhao, “Non-linear tip speed ratio cascade control for variable speed high power wind turbines: a backstepping

approach", *IET Renewable Power Generation*, 2018, 12(8): 968-972.
[24] J. A. Farrell, M. Polycarpou, M. Sharma, et al, "Command filtered backstepping", *IEEE Transactions on Automatic Control*, 2009, 54(6): 1391-1395.
[25] G. Cui, S. Xu, F. L. Lewis, et al, "Distributed consensus tracking for non-linear multi-agent systems with input saturation: a command filtered backstepping approach", *IET Control Theory & Applications*, 2016, 10(5): 509-516.
[26] Y. Pan, H. Wang, X. Li, et al, "Adaptive Command-Filtered Backstepping Control of Robot Arms With Compliant Actuators", *IEEE Transactions on Control Systems Technology*, 2018, 26(3): 1149-1156.
[27] Q. Zhou, H. Li and P. Shi, "Decentralized Adaptive Fuzzy Tracking Control for Robot Finger Dynamics", *IEEE Transactions on Fuzzy Systems*, 2015, 23(3): 501-510.
[28] S. Tong, Y. Li and P. Shi, "Observer-Based Adaptive Fuzzy Backstepping Output Feedback Control of Uncertain MIMO Pure-Feedback Nonlinear Systems", *IEEE Transactions on Fuzzy Systems*, 2012, 20(4): 771-785.
[29] M. I. Ghiasi, M. A. Golkar and A. Hajizadeh, "Lyapunov Based-Distributed Fuzzy-Sliding Mode Control for Building Integrated-DC Microgrid With Plug-In Electric Vehicle", *IEEE Access*, 2017, 5:7746-7752.
[30] G. C. Hsieh, H. I. Hsieh, C. Y. Tsai, et al, "Photovoltaic Power-Increment-Aided Incremental-Conductance MPPT With Two-Phased Tracking", *IEEE Transactions on Power Electronics*, 2013, 28(6): 2895-2911.
[31] A. Ajami, A. M. Shotorbani and M. P. Aagababa, "Application of the direct Lyapunov method for robust finite-time power flow control with a unified power flow controller", *IET Generation, Transmission & Distribution*, 2012, 6(9): 822-830.
[32] Q. Shen, P. Shi and Y. Shi, "Distributed Adaptive Fuzzy Control for Nonlinear Multiagent Systems Via Sliding Mode Observers", *IEEE Transactions on Cybernetics*, 2016, 46(12): 3086-3097.
[33] W. X. Yan, J. Huang, and D. Z. Xu, "Adaptive command-filtered backstepping control for linear induction motor via projection algorithm", *Mathematical Problems in Engineering*, 2016: 1-13.
[34] Z. Cai, M. S. De Queiroz, and D. M. Dawson, "A sufficiently smooth projection operator", *IEEE Transactions on Automatic Control*, 2006, 51(1): 135C139.